

Faraday Discussions

Accepted Manuscript



This manuscript will be presented and discussed at a forthcoming Faraday Discussion meeting. All delegates can contribute to the discussion which will be included in the final volume.

Register now to attend! Full details of all upcoming meetings: <http://rsc.li/fd-upcoming-meetings>



This is an *Accepted Manuscript*, which has been through the Royal Society of Chemistry peer review process and has been accepted for publication.

Accepted Manuscripts are published online shortly after acceptance, before technical editing, formatting and proof reading. Using this free service, authors can make their results available to the community, in citable form, before we publish the edited article. We will replace this *Accepted Manuscript* with the edited and formatted *Advance Article* as soon as it is available.

You can find more information about *Accepted Manuscripts* in the [Information for Authors](#).

Please note that technical editing may introduce minor changes to the text and/or graphics, which may alter content. The journal's standard [Terms & Conditions](#) and the [Ethical guidelines](#) still apply. In no event shall the Royal Society of Chemistry be held responsible for any errors or omissions in this *Accepted Manuscript* or any consequences arising from the use of any information it contains.

Changing the Magnetic Properties of Microstructure by Directing the Self-assembly of Superparamagnetic Nanoparticles

Suvojit Ghosh^a and Ishwar K. Puri^{*a, b}

5 DOI: 10.1039/b000000x [DO NOT ALTER/DELETE THIS TEXT]

Magnetic nanoparticles (MNPs) in a liquid dispersion can be organized through controlled self-assembly by applying an external magnetic field that regulates inter-particle interactions. Thus, micro- and nanostructures of desired morphology and superlattice geometry that show emergent magnetic properties can be fabricated. We describe how superferromagnetism, which is a specific type of emergence, can be produced. Here, superparamagnetic nanoparticles that show no individual residual magnetization are organized into structures with substantial residual magnetization that behave as miniature permanent magnets. We investigate the emergence of superferromagnetism in an idealized system consisting of two MNPs by considering the influence that interparticle magnetostatic interactions have on the dynamics of the magnetic moments. We use this model to illustrate the design principles for self-assembly in terms of the choice of material and MNP particle size. We simulate the dynamics of the interacting magnetic moments by applying the stochastic Landau-Lifshitz-Gilbert equation to verify our principles. The findings enable a method to pattern material magnetization with submicron resolution, a useful feature that has potential applications for magnetic recording and microfluidic particle traps. The analysis also yields useful empirical generalizations that could facilitate other theoretical developments.

1 Introduction

Magnetic nanoparticles (MNPs) are excellent building blocks, using which features at the nano or microscale can be fabricated bottom-up. The self-assembly and geometric organization of superparamagnetic MNPs can be controlled with an external magnetic field which regulates their interparticle magnetostatic interactions. This self-assembly process has two main features. First, inter-particle 'bonds' align with the direction of the field,¹⁻³ and, next, their magnetostatic interactions are turned 'on' or 'off'.^{4,5} Thus, using a specific magnetic field, microstructures of various shapes and sizes can be fabricated⁶⁻⁸ and different geometries can be enforced for the MNP superlattice.⁹⁻¹¹ Since the bulk properties of a material containing these structures, e.g., in polymer-MNP composites, depend on the geometric organization of MNPs in the surrounding matrix, this leads to prospects for material design.^{6, 12-14} Our focus is on how the magnetic properties of such microstructures can be designed.

To control the self-assembly of MNPs, it is essential to begin with a stable colloidal dispersion in which particle aggregation is minimal, i.e., in which inter-particle magnetostatic interactions have been minimized.¹⁵ This is accomplished by using superparamagnetic⁴ MNPs, since the frequent thermally-driven reversals of their

magnetic moments \mathbf{m} render a zero effective moment on the timescale of particle transport.¹⁶⁻¹⁸ While the colloidal dispersions are typically dilute, the magnetic field-assisted self-assembly brings the MNPs into close proximity. Consequently, the magnetostatic interactions among the magnetic moments of neighboring particles become significant, which influences the dynamics of the moments.¹⁹ We explore how these interactions can lead to a non-zero residual magnetization in a bulk structure formed through the self-assembly of superparamagnetic MNPs. This residual magnetization, or superferromagnetism,²⁰ emerges when the interparticle magnetostatic interactions present an energy barrier E_b to the reversals in \mathbf{m} , one that frequently cannot be overcome by thermal fluctuations. As a result the moments for individual MNPs in the structure remain stable in their orientation so that the structure develops a residual magnetization.

Nano- and microscale structures with residual magnetization have several potential uses. Self-assembly is an inexpensive alternative to their current fabrication with methods such as machining²¹ and lithography.²² Residual magnetization enables data storage in magnetic recording media, since reducing the size of a single data bit to a few nanoparticles enhances data density.²³ Because the formed structures are miniature permanent magnets, they produce strong localized magnetic field gradients that can influence particle transport in liquid suspensions, e.g., for biomedical applications such as cell sorting^{24, 25} and trapping,^{21, 26} and manufacturing approaches for pattern transfer from a template.^{22, 27} Since MNP self-assembly can be performed *in situ* during the solution-casting of polymers, the ensuing microstructures can be readily embedded into the architecture of microfluidic devices, e.g., ones made out of PDMS.^{7, 28, 29}

The simplest microstructure produced by the magnetic field-directed self-assembly of superparamagnetic MNPs occurs as a linear chain.^{1, 6} If the magnetocrystalline easy axes \mathbf{n}_i of each MNP in such a chain lie parallel to the chain direction, residual magnetization can emerge.^{19, 20} This outcome arises only when inter-particle magnetostatic interactions augment E_b to such a high level that this energy barrier cannot be typically overcome by the thermal fluctuations in the particle magnetic moments. The simplest manifestation of this effect is shown in the two-particle-system (TPS) of Figure 1a. The model, although idealized, is one that allows fundamental theoretical study of the dynamics of interacting moments by examining the influence of magnetostatic interactions on the reversal trajectory of \mathbf{m} and the associated energy cost E_b .^{23, 30-34}

For our self-assembly problem where microstructures with residual magnetization are produced in a liquid dispersion of superparamagnetic MNPs, we identify (1) a necessary particle size window, and (2) a dimensionless number involving two MNP properties, their saturation magnetization M_s and magnetocrystalline anisotropy constant K , that can be used to determine the suitability of an MNP material. We verify our findings with micromagnetics simulations where the trajectories of interacting magnetic moments are calculated using a stochastic form of the Landau-Lifshitz-Gilbert (LLG)^{35, 36} equation that incorporates the effects of thermal fluctuations.^{32, 37-39} We also report a significant empirical generalization that could lead to future theoretical studies.

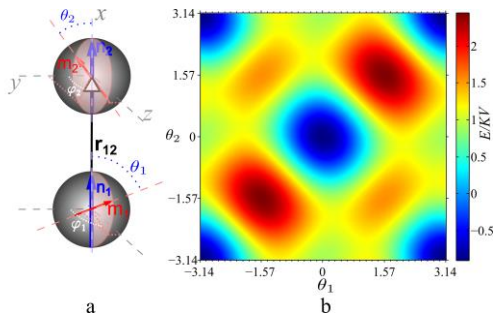


Figure 1 (a) A system of two MNPs with their magnetocrystalline easy axes \mathbf{n}_1 and \mathbf{n}_2 parallel to the ‘bond’ direction \mathbf{r}_{12} . The magnetic moments \mathbf{m}_1 and \mathbf{m}_2 can rotate with respect to the particles at the cost of the total potential energy E described in Equation 5. (b) The map of $E(\theta_1, \theta_2)$ in the plane of $\varphi_1 = \varphi_2$ shows that equilibria of the \mathbf{m}_i are located at $\theta_i = \theta_2 = 0, \pm\pi$, i.e., the \mathbf{m}_i are parallel to each other as well as to $\pm\mathbf{r}_{12}$. Only the $\varphi_1 = \varphi_2$ plane is shown because the equilibria and the minimum energy barriers between them are all contained by this plane.

Table 1 Nomenclature

Symbol	Quantity	Dimensions	Units
a	Particle radius	[L]	m
\mathbf{B}	Magnetic Field	[M][T] ⁻² [I] ⁻¹	T
\mathbf{e}	Non-dimensional magnetic moment defined as $\mathbf{e} = \mathbf{m}/ \mathbf{m} $	-	dimensionless
f	Magnetization reversal frequency	[T] ⁻¹	Hz
f_0	Attempt frequency	[T] ⁻¹	Hz
E	Potential energy of a system of magnetic nanoparticles	[M][L] ² [T] ⁻²	J
E_a	Anisotropy energy	[M][L] ² [T] ⁻²	J
E_b	Energy barrier for magnetization reversal	[M][L] ² [T] ⁻²	J
k_B	Boltzmann constant	[M][L] ² [T] ⁻² [θ] ⁻¹	J K ⁻¹
k_{int}	Dipolar interaction strength defined by Equation (5)	-	dimensionless
K	Magnetocrystalline anisotropy constant	[M][L] ⁻¹ [T] ⁻²	J m ⁻³
K_{eff}	Effective anisotropy constant defined by Equation (7)	[M][L] ⁻¹ [T] ⁻²	J m ⁻³
\mathbf{m}	Magnetic moment	[L] ² [I]	A m ⁻²
M_s	Saturation Magnetization	[L] ⁻¹ [I]	A m ⁻¹
\mathbf{n}	Direction of easy axis	-	dimensionless
r	Inter-particle distance	[L]	m
T	Temperature	[θ]	K
V	Particle volume	[L] ³	m ³
γ	Gyromagnetic constant	[M] ⁻¹ [T] ¹ [I] ¹	T ⁻¹ s ⁻¹
λ	Damping Constant	-	dimensionless
μ_0	Permeability of free space	[M][L][T] ⁻² [I] ⁻²	N A ⁻²
τ_m	Measurement time	[T]	s

2 Theory and Analysis

2.1 Theory

¹⁰ An MNP is superparamagnetic if its magnetic moment \mathbf{m} undergoes several thermally driven reversals over the time period of measurement τ_m , i.e., $\tau_m \gg f^{-1}$ where f represents the frequency of reversals. This is because the time-average of \mathbf{m} over τ_m ,

$|\langle \mathbf{m} \rangle| \ll |\mathbf{m}|$, i.e., the particle shows zero effective residual magnetization. On the other hand, the MNP is ferromagnetic if there are very few reversals over the measurement interval, i.e., $\tau_m \ll f^{-1}$ as $|\langle \mathbf{m} \rangle| \approx |\mathbf{m}|$, i.e., the MNP exhibits residual magnetization. The reversal frequency can be predicted by the Néel-Arrhenius relation,⁴⁰

$$f = f_0 \exp\left(-\frac{E_b}{k_B T}\right), \quad (1)$$

where E_b denotes the potential energy barrier for the reversals and $f_0 \sim 10^9 - 10^{11}$ Hz is the attempt frequency.^{32, 39, 41} We can examine the emergence of superferromagnetism if we are able to determine how E_b is influenced by magnetostatic interactions.

The magnetic moment of an MNP has an inherent predilection to align itself with the magnetocrystalline easy-axes, which are the preferred crystallographic directions fixed to the MNP. For simplicity, we consider the case of uniaxial anisotropy, i.e., each MNP possesses a single easy axis, \mathbf{n} . Misalignment between \mathbf{m} and \mathbf{n} occurs at the cost of the anisotropy energy,

$$E_a = -\frac{KV}{|\mathbf{m}|^2} (\mathbf{m} \cdot \mathbf{n})^2, \quad (2)$$

where K denotes the magnetocrystalline anisotropy constant and V the particle volume. Thus, for an isolated MNP, in the absence of a magnetic field, the energy barrier for the reversal of \mathbf{m} is $E_b = KV$. When other MNPs are present in close proximity, the consideration is more complicated. In a system of MNPs, the i^{th} particle encounters the magnetic field,

$$\mathbf{B}_i^{\text{dip}} = \frac{\mu_0}{4\pi} \sum_{j \neq i} \left(\frac{3\mathbf{r}_{ij}(\mathbf{r}_{ij} \cdot \mathbf{m}_j)}{r_{ij}^5} - \frac{\mathbf{m}_j}{r_{ij}^3} \right), \quad (3)$$

due to its neighbors, where \mathbf{r}_{ij} denotes the position vector of the i^{th} particle relative to the j^{th} particle and \mathbf{m}_j is the j^{th} particle's magnetic moment. This field is responsible for magnetostatic interactions between the moments of neighboring MNPs. The Zeeman energy of a dipole in a magnetic field \mathbf{B} is $E = -\mathbf{m} \cdot \mathbf{B}$. Thus, the total energy for a system of particles is the sum of the anisotropy energies for each particle E_a added to the sum of the Zeeman energies for all particle pairs E_{dip} ,

$$E = E_a + E_{\text{dip}} = -\sum_i \frac{KV}{|\mathbf{m}_i|^2} (\mathbf{m}_i \cdot \mathbf{n}_i)^2 + \frac{\mu_0}{4\pi} \sum_{i>j} \left(\frac{\mathbf{m}_i \cdot \mathbf{m}_j}{r_{ij}^3} - 3 \frac{(\mathbf{m}_i \cdot \mathbf{r}_{ij})(\mathbf{m}_j \cdot \mathbf{r}_{ij})}{r_{ij}^5} \right). \quad (4)$$

For a TPS, this expression can be simplified as,

$$\frac{E}{KV} = -\sum_i (\hat{\mathbf{e}}_i \cdot \hat{\mathbf{n}}_i)^2 + k_{\text{int}} (\hat{\mathbf{e}}_1 \cdot \hat{\mathbf{e}}_2 - 3(\hat{\mathbf{e}}_1 \cdot \hat{\mathbf{e}}_r)(\hat{\mathbf{e}}_2 \cdot \hat{\mathbf{e}}_r)), \quad (5)$$

where $\hat{\mathbf{e}}_i = \mathbf{m}_i / |\mathbf{m}_i|$, $\hat{\mathbf{e}}_r = \mathbf{r}_{ij} / |\mathbf{r}_{ij}|$, and, for closely packed structures with $r \sim 2a$, the dipolar interaction strength $k_{\text{int}} = \mu_0 M_s^2 / 24K$ is independent of particle radius a . For our model system of two particles illustrated in Figure 1a, the resulting energy map is presented in Figure 1b, which shows that the equilibria for this system requires that $\mathbf{m}_1 + \mathbf{m}_2$ be parallel or anti-parallel to \mathbf{r}_{12} . Thus, it is a two-well system similar to the isolated MNP described in Equation (2).

2.2 The potential barrier of a two-particle-system

The energy map for a TPS has a significant difference from that for a single particle. For an isolated MNP the energy map is one-dimensional, i.e., $E = E(\theta)$ where $\theta = (\mathbf{m} \cdot \mathbf{n}) / |\mathbf{m} \cdot \mathbf{n}|$. Thus, it has a unique potential barrier KV separating the two wells. Whenever thermal fluctuations provide energy greater than KV , the moment can switch between the two states. For the TPS, $E = E(\theta_1, \theta_2, \varphi_1, \varphi_2)$ and the energy cost of switching between the two states is path dependent, i.e., an unique E_b is not defined. We will first verify that Equation (1) is valid for a TPS in Section 3.1. Next, we will determine the effective barrier E_b^{eff} that enables calculation of the reversal frequency f from Equation (1).

The calculation of E_b^{eff} can be accomplished numerically using the stochastic micromagnetics simulations, as shown in Section 3.1. However, we require an analytical formulation for a potential barrier in order to develop design principles. Thus, we select the saddle points in the energy map of Equation (5) E_b^{sad} to calculate the reversal frequency from Equation (1). This is because E_b^{sad} is the lowest barrier between the two wells for a TPS, i.e., $E_b^{\text{sad}} < E_b^{\text{eff}}$. Thus, from Equation (1), when f is calculated using E_b^{sad} it is necessarily greater than when E_b^{eff} is used. A two-particle-system that is predicted to be superferromagnetic using E_b^{sad} will also lead to the same prediction if E_b^{eff} were used instead. For strong interparticle magnetostatic interactions and in the absence of an externally applied magnetic field, the barriers corresponding to these saddle points are³⁴

$$E_b^{\text{sad}} = 2KV \left(1 + \frac{k_{\text{int}}}{2} \right). \quad (6)$$

2.3 The effective anisotropy constant

For an isolated particle, $E_b = KV$. Thus, the reversal frequency is given by $f = f_0 \exp(-KV/k_b T)$. Drawing an analogy with the TPS, we define an effective anisotropy constant K_{eff} , such that $E_b^{\text{sad}} = K_{\text{eff}} V$. Thus, K_{eff} can be used in the single-particle form of the Néel-Arrhenius relation, i.e., $f = f_0 \exp(-K_{\text{eff}} V / k_b T)$. From Equation (6),

$$K_{\text{eff}} = 2K \left(1 + \frac{k_{\text{int}}}{2} \right). \quad (7)$$

This step is purely for convenience in analysis and is similar to the concept of an effective volume.⁴²

3 Results and Discussions

3.1 Determining the potential barrier in a two-particle-system (TPS)

We first verify that the frequency of magnetization reversal in a TPS obeys the Néel-Arrhenius relation in Equation (1). This is accomplished by simulating the dynamics of the magnetic moments of an isolated particle ($N = 1$) and a TPS ($N = 2$) using the stochastic LLG equations. The reversal frequency f decays exponentially with $1/T$ for both systems, as seen in Figure 2. This verifies that the Néel-Arrhenius relation is followed and that we can determine when a system of MNPs transitions from superparamagnetic behavior to superferromagnetic behavior entirely by calculating the changes in its energy barrier.

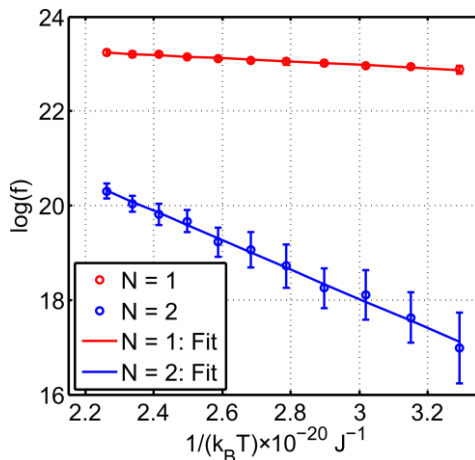


Figure 2 Exponential decay of reversal frequency f with $1/(k_B T)$ for magnetite particles with $a = 3.5$ nm verifies that the Néel-Arrhenius relation is followed for both an isolated MNP ($N = 1$) and the two-particle-system ($N = 2$). The slope of the line is used to calculate the effective potential barrier E_b^{eff} . Each data point is generated from the trajectory of \mathbf{m}_i for 10 intervals of 100 ns. Table 2 compares numerical results with the theoretical estimates.

Table 2 Comparison of the numerically determined E_b^{eff} with the theoretical predictions

	$N = 1$	$N = 2$
E_b^{eff} / KV (Numerical)	0.839	7.524
E_b^{sad} / KV (Theoretical)*	1.000	2.453

*For an isolated particle ($N = 1$), no saddle points exist and $E_b^{\text{sad}} = KV$ as seen in Equation (2).

Next, we determine E_b^{eff} from numerical simulations and compare the values to the barriers posed by saddle points in the energy map described by Equation (6). This is done by fitting a straight line to the $\log(f) - 1/k_B T$ relation of Figure 2. The slope of the line yields E_b^{eff} . The values obtained are presented in Table 2 and compared with theoretical predictions, i.e., $E_b = KV$ for isolated particles ($N = 1$) and $E_b^{\text{sad}} = 2KV(1 + k_{\text{int}}/2)$ for the TPS ($N = 2$). For $N = 1$, E_b is expected to be underestimated since \mathbf{m} seldom relaxes to an equilibrium state that is aligned with the easy axis \mathbf{n} . The energy expense for a reversal is therefore rarely equal to the theoretical barrier of KV . For $N = 2$, while, the disparity is much larger, $E_b^{\text{eff}} > E_b^{\text{sad}}$ as predicted in Section 2.2.

3.2 Choice of particle size

We now determine the bounds on the particle size window within which, over a duration τ_m , (1) an isolated MNP has frequent reversals in its magnetic moment \mathbf{m} due to the relatively low energy barrier that opposes thermally driven reversals, and (2) when two of the same MNPs are assembled into a TPS, as seen in Figure 1a, magnetostatic interactions among their moments enhance the barrier to a value that is sufficient to prevent frequent reversals. Thus, within this particle size window, an isolated MNP has negligible residual magnetic moment over the measurement interval τ_m , i.e., the time-average of the x -component of the normalized magnetic moment in

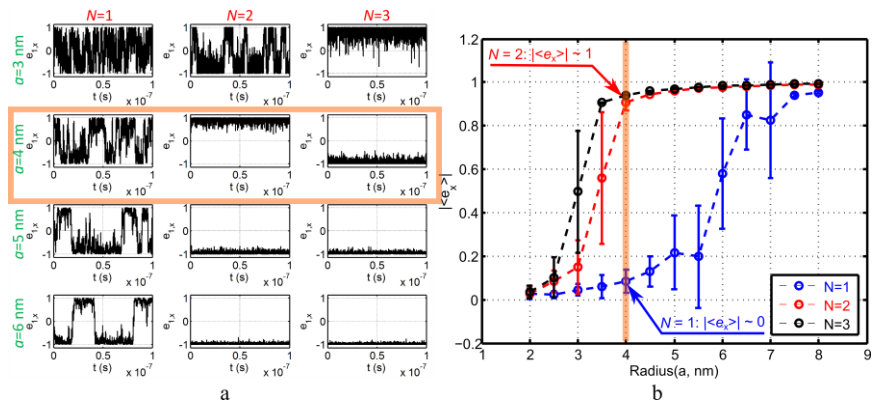


Figure 3 (a) The time-series of the x -component of dimensionless magnetic moment e_x for an isolated MNP ($N = 1$), a TPS ($N = 2$), and a longer chain ($N = 3$) of magnetite nanoparticles at $T = 300\text{K}$ over a $\tau_m = 100$ ns interval shows that a chain of MNPs always has a smaller number of reversals. (b) The time average of the dimensionless magnetic moment $\langle e_x \rangle$ obtained from 10 such simulations shows that within a window of particle sizes, an isolated MNP exists in superparamagnetic state with $\langle e_x \rangle \ll 1$ whereas a TPS shows residual magnetization with $\langle e_x \rangle \approx 1$. The red box and red line demonstrates this for particles with radius $a = 4$ nm.

Table 3 Material properties of common MNP materials from Ref. 43 and the calculated bounds for the particle size window. When particle radius $a \in (a_1, a_2)$, an isolated MNP has zero residual magnetization while a two-particle-system develops residual magnetization for a measurement time $\tau_m = 100$ ns at $T = 300$ K.

Material	M_s (kA/m)	K (kJ/m ³)	a_1 $KV \sim 8k_B T$ (nm)	a_2 $K_{eff} V \sim 8k_B T$ (nm)
Magnetite	446	23	7	5.2
fcc FePt	1140	206	3.4	2.5
Maghemite	414	4.7	11.9	7.5
FeCo	1790	1.5	17.4	3.6
CoFe ₂ O ₄	425	180	3.5	2.8
BaFe ₂ O ₄	380	300	3.0	2.3

this interval $\langle e_x \rangle \ll 1$. However, a TPS has a residual magnetization with $\langle e_x \rangle \approx 1$. This transition and the existence of the bounds on particle radius a are illustrated in Figure 3.

Since magnetite forms the core of many commercially available MNPs, we use it as an example material in our analysis. Magnetite has a saturation magnetization $M_s = 446 \times 10^3$ A/m and an anisotropy constant $K = 23 \times 10^3$ J/m³.⁴³ Thus, the energy barrier separating the two stable equilibria of \mathbf{m} in an isolated magnetite nanoparticle arises solely due to magnetocrystalline anisotropy, i.e., $E_b = KV = 9.63a^3 \times 10^4$ J. We first estimate the largest particle radius a_1 for which an isolated magnetite MNP is superparamagnetic over a measurement time $\tau_m = 100$ ns. This requires that its moments reverse multiple times over $\tau_m = 100$ ns, i.e., $f \geq 10^7$ Hz. Assuming $f_0 \sim 30$ GHz⁴¹ and using Equation (1), the energy barrier $E_b \leq 8k_B T$, i.e., at $T = 300$ K, $a_1 \approx 7$ nm. For any isolated magnetite MNP with $a \leq a_1$, the moment undergoes magnetization reversals over 100 ns. As seen in Figure 3a, for $a = 6$ nm and $N = 1$, a few magnetization reversals are observed. This yields a zero residual magnetization over $\tau_m = 100$ ns, i.e., $\langle e_x \rangle \ll 1$, confirmed in Figure 3b.

Similarly, we can evaluate the smallest particle radius a_2 for which a TPS demonstrates superferromagnetism over the same time interval. Here, we assume the potential barrier is enhanced to $E_b = 2KV(1 + k_{int}/2) = K_{eff}V$ as per the discussion in Section 2.2, and that the relation $E_b \geq 8k_B T$ holds for a TPS as well. This yields $a_2 = 5.20$ nm, i.e., a TPS where particles have $a \geq a_2$ yields residual magnetization over 100 ns. We observe from Figure 3a that when $N = 2$ and $a \geq 4$ nm, the system has a fairly stable magnetization. The mismatch is explained by the fact that $E_b^{sad} < E_b^{eff}$ as discussed in Section 2.2 and verified in Section 3.1. This yields a substantial residual magnetization over $\tau_m = 100$ ns, i.e., $\langle |e_x| \rangle \approx 1$, as confirmed in Figure 3b. This analysis is strictly true only if f_0 is identical for both $N = 1$ and 2, which is not always the case. However, considering that $a_2 = (\ln(f_0 \tau_m) \times 3 / 4\pi \times 8k_B T / K_{eff})^{1/3}$, i.e. $a_2 \sim (\ln(f_0))^{1/3}$ and the attempt frequencies differ by less than an order of magnitude as listed in Table 4, such an assumption is plausible.

From these two considerations, for a duration of $\tau_m = 100$ ns and at $T = 300$ K, all particle sizes within $a_1 > a > a_2$ have no net magnetization when isolated, i.e., existing as a dilute dispersion. However, when they are self-assembled to form a linear chain having aligned easy axes, a residual magnetization is observed over τ_m . The same analysis can be undertaken for any MNP material provided the values of K and M_s are accurately known. Table 3 lists the two critical radii determined from similar considerations for a wide range of MNP materials.

3.3 Choice of particle material

While designing a self-assembly process, a metric that evaluates the suitability of a material is useful. Because synthesis processes for MNPs lead to polydispersity in particle size, an MNP material is better suited than another if the acceptable particle size window for that material is wider, i.e., the ratio a_1 / a_2 for the material is larger. The exact bounds on the particle radii window depend on the choice of τ_m and temperature T . However, the ratio a_1 / a_2 depends solely on the material properties, i.e. on the saturation magnetization M_s and anisotropy constant K . Following the analysis in Section 3.2, $a_1 / a_2 = K_{eff} / K$. Thus, from Equation (7),

$$\frac{a_1}{a_2} = (2 + k_{int})^{1/3}. \quad (8)$$

Figure 4 plots Equation (8) and also identifies where the materials listed in Table 3 are located on it. Larger values of k_{int} allow a wider particle radii window for the self-assembly process. Thus, materials with larger M_s and lower K are better suited for self-assembly processes that organize superparamagnetic nanoparticles to yield superferromagnetism, since a higher M_s yields greater strength for inter-particle magnetostatic interactions while a smaller K provides a lower barrier of magnetization reversal for isolated particles. Thus, raising M_s increases a_1 while lowering K decreases a_2 .

3.4 Longer chains ($N > 2$)

Linear chains formed by self-assembled MNPs are seldom two particles long. Thus, we consider the implications of our design process on longer chains. The analytical formulation of the potential barrier, even with simplifying assumptions, e.g., the use of the saddle points in the energy map, are not possible for $N > 2$. Thus, we resort to observations in the dynamics of the magnetic moments simulated using the LLG

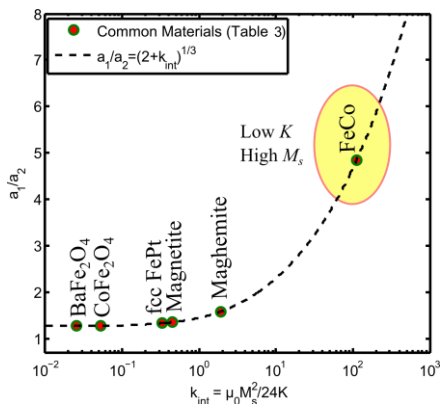


Figure 4 The ratio of the bounds on the window of particle sizes a_1/a_2 within which an isolated MNP is superparamagnetic, but a two-particle-system demonstrates superferromagnetism, increases monotonically with the interaction strength $k_{int} = \mu_0 M_s^2 / 24K$. Thus, a material with a higher k_{int} has a wider window and is better suited to a self-assembly process that will yield superferromagnetism. equations.

Figure 5 shows that f decays exponentially with MNP volume V for the chain lengths considered. Thus, the Néel-Arrhenius relation of Equation (1) is satisfied and a value for the effective anisotropy constant K_{eff}^{num} can be calculated from the slope of the $\log(f) - V$ plots. The attempt frequency f_0 can also be determined from the y-intercept of the plots. The values of both these metrics are presented in Table 4. For the isolated MNP, the calculated K_{eff}^{num} is exactly equal to the anisotropy constant of magnetite, the MNP material for which these simulations were conducted. A significant observation from Figure 5 is that longer chains have a lower reversal frequency unless the particle volume is extremely small. Thus, if a self-assembly process is designed to produce superferromagnetism using the idealized TPS model developed herein, it will assuredly produce superferromagnetism for the longer chains that are actually produced for most MNP sizes. This lower limit on MNP size is unrealistically small, as explained below.

3.5 Empirical generalization: an universal attempt frequency

Another observation from Figure 5 and Table 4 is that the attempt frequency f_0 varies significantly with chain length N . The nature of the lines indicates that an exponential relation of the form,

$$f = f_0 \exp\left(-\frac{K_{eff}(V - V_0)}{k_B T}\right), \tag{9}$$

is an effective replacement for Equation (1) for a system of interacting MNPs in a linear chain. This empirically derived expression allows us to employ a simplified universal value of f_0 for interacting MNPs. The theoretical basis for this expression is outside the scope of this work.

We note here that the design principles developed above are only valid for particles when $V > V_0$. This is because when $V < V_0$, the reversal frequency of an isolated particle is smaller than for a TPS, and that for a TPS is smaller than any of the longer chains, as seen from Figure 5. However, almost all realistic MNPs have larger volumes

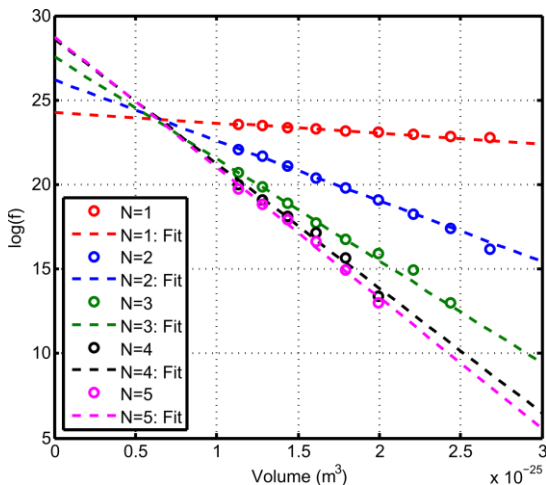


Figure 5 The reversal frequency f decays exponentially with MNP volume in an isolated MNP as well as the linear chains of various lengths. The slope of the curve allows K_{eff}^{num} to be determined, while the y-intercept provides the value of the attempt frequency f_0 (Table 4). Each data point is the mean value realized from 10 simulations of 1 μ s duration for magnetite nanoparticles.

Table 4 The effective anisotropy constant K_{eff}^{num} and the attempt frequency f_0 calculated from simulation data presented in Figure 5 for magnetite nanoparticles.

Chain Length (N)	K_{eff} from Eq. (7) (kJ m^{-3})	K_{eff}^{num} from Fig. 5 (kJ m^{-3})	f_0 (GHz)
1	23.0*	23.0	31.8
2	56.4	146.3	223.4
3	-	-	601.2
4	-	306.1	2742.2
5	-	324.0	3106.4

*The effective anisotropy constant of a single particle is simply magnetocrystalline anisotropy constant of the material K . The corresponding numerical value shows good agreement.

than the V_0 observed here, which corresponds to particles with a radius $a \approx 2$ nm.

10 4 Computational Method

Micromagnetics simulations using the stochastic Landau-Lifshitz-Gilbert (LLG) equation^{36, 44} provide the magnetic properties of a system of MNPs by simulating the dynamics of the magnetic moment of each participating MNP.^{38, 41, 45} Due to the presence of a single domain in an MNP and the consequent coherence among the moments of the individual atoms comprising it, the magnetization of a particle can be considered as a single magnetic moment \mathbf{m} .⁴⁶ This macrospin approximation simplifies the use of the LLG equation^{36, 44} to predict the dynamics of the magnetic moment of an MNP.^{37, 47-49} Its stochastic form is a Langevin equation,³⁷

$$\frac{d\mathbf{m}_i}{dt} = \gamma \mathbf{m}_i \times (\mathbf{B}_i^{eff} + \mathbf{b}_\beta) - \frac{\gamma\lambda}{m_i} \mathbf{m}_i \times (\mathbf{m}_i \times (\mathbf{B}_i^{eff} + \mathbf{b}_\beta)), \quad (10)$$

20 where γ denotes the gyromagnetic constant of an electron spin, and λ is a phenomenological damping constant.^{37, 47} $\mathbf{B}_i^{eff} = \mathbf{B}_i^{dip} + \mathbf{B}_i^a + \mathbf{B}_i^{ex}$ denotes the total

effective field on the i^{th} particle while $\mathbf{B}_i^a = (2KV / m^2)(\mathbf{m} \cdot \mathbf{n})\mathbf{n}$ models the effect of magnetocrystalline anisotropy and $\mathbf{B}_i^{\text{ext}}$ is the externally applied field, which is assumed zero for our purpose. We use a time step $\Delta t = 10^{-12}$ s for which thermal agitation can be modeled as a purely random process.^{46, 50} This implies that thermal fluctuations in \mathbf{m} can be investigated as the effect of a magnetic field \mathbf{b}_β that satisfies the properties of a Gaussian stochastic process,^{37, 47}

$$\langle b_{\beta,\alpha}(t) \rangle = 0; \quad \langle b_{\beta,\alpha}(t)b_{\beta,\beta}(s) \rangle = 2 \frac{\lambda}{1+\lambda^2} \frac{k_B T}{\gamma m} \delta_{\alpha\beta} \delta(t-s). \quad (11)$$

A stochastic form of the Heun scheme is used to integrate Eq. (10), an approach that is consistent in the sense of Stratonovich stochastic calculus.³⁷ This assumption and the time step value are justified by a general response time for a single domain particle that is of the order of 10^{-10} s.⁴⁶

5 Conclusions

The magnetic field-controlled self-assembly of MNPs can generate microstructures of various forms. However, good control over this form of self-assembly requires that particles are superparamagnetic so as to avoid aggregation by magnetostatic interactions. We develop the design principles of a self-assembly process wherein superparamagnetic nanoparticles, which have zero residual magnetization individually, are organized into microstructures that demonstrate a residual magnetization. To do so, we consider the influence of inter-particle magnetostatic interactions on the potential barrier for magnetization reversals in an idealized system comprised of two MNPs. The principles developed herein enable the proper selection of MNPs of requisite sizes and materials such that the microstructures are able to develop residual magnetization, potentially impacting a large number of applications, e.g., magnetic data storage and microfluidic particle traps. Since self-assembly can be a relatively inexpensive and more effective fabrication method, it offers an alternative to current techniques, such as sophisticated machining or lithography. Our analytical methods could pave the way for the design of other self-assembly processes that produce emergent magnetic properties in microstructures.¹⁹

Acknowledgements

The Virginia Tech Advanced Research Computing cluster ATHENA and the Department of Engineering Science and Mechanics Linux Compute Cluster were used for the simulations.

References

- ^a Department of Engineering Physics, McMaster University, Hamilton, Ontario, Canada. Tel: 905-525-9140; E-mail: sghosh@mcmaster.ca
- ^b Department of Mechanical Engineering, McMaster University, Hamilton, Ontario, Canada. Tel: 905-525-9140; E-mail: ikpuri@mcmaster.ca
1. K. Butter, P. H. H. Bomans, P. M. Frederik, G. J. Vroege and A. P. Philipse, *Nat. Mater.*, 2003, 2, 88-91.
2. G. Bertoni, B. Torre, A. Falqui, D. Fragouli, A. Athanassiou and R. Cingolani, *J. Phys. Chem. C*, 2011, 115, 7249-7254.
3. Y. Lalatonne, J. Richardi and M. P. Pileni, *Nat Mater*, 2004, 3, 121-125.

4. C. P. Bean and J. D. Livingston, *J. Appl. Phys.*, 1959, 30, S120-S129.
5. R. Ganguly and I. Puri, *Advances in applied mechanics*, 2007, 41, 293-335.
6. D. Fragouli, R. Buonsanti, G. Bertoni, C. Sangregorio, C. Innocenti, A. Falqui, D. Gatteschi, P. D. Cozzoli, A. Athanassiou and R. Cingolani, *ACS Nano*, 2010, 4, 1873-1878.
7. S. Ghosh and I. K. Puri, *Soft Matter*, 2013, 9, 2024-2029.
8. W. K. Lee, *J. Magn. Magn. Mater.*, 2010, 322, 2525-2528.
9. A. Goyal, C. K. Hall and O. D. Velev, *J. Chem. Phys.*, 2010, 133.
10. J. Legrand, A. T. Ngo, C. Petit and M. P. Pileni, *Advanced Materials*, 2001, 13, 58-62.
11. A. Ahniyaz, Y. Sakamoto and L. Bergström, *Proceedings of the National Academy of Sciences*, 2007, 104, 17570-17574.
12. A. S. Robbes, F. Cousin, F. Meneau, F. Dalmas, F. Boue and J. Jestin, *Macromolecules*, 2011, 44, 8858-8865.
13. D. Fragouli, A. Das, C. Innocenti, Y. Guttikonda, S. Rahman, L. Liu, V. Caramia, C. M. Megaridis and A. Athanassiou, *ACS Applied Materials & Interfaces*, 2014, 6, 4535-4541.
14. Z. Varga, G. Filipcsei and M. Zrínyi, *Polymer*, 2006, 47, 227-233.
15. R. E. Rosensweig, *Ferrohydrodynamics*, Dover Publications, 1997.
16. R. Ganguly and I. K. Puri, *Advances in Applied Mechanics*, 2007, 41, 293-335.
17. R. Ganguly, B. Zellmer and I. K. Puri, *Phys. Fluids*, 2005, 17, 097104.
18. R. Ganguly, A. P. Gaiind and I. K. Puri, *Physics of Fluids*, 2005, 17.
19. B. Subhankar and K. Wolfgang, *J. Phys. D: Appl. Phys.*, 2009, 42, 013001.
20. S. Mørup, *Hyperfine Interact.*, 1994, 90, 171-185.
21. K. Ino, M. Okochi, N. Konishi, M. Nakatochi, R. Imai, M. Shikida, A. Ito and H. Honda, *Lab Chip*, 2007, 8, 134-142.
22. J. Henderson, S. Shi, S. Cakmaktepe and T. Crawford, *Nanotechnology*, 2012, 23, 185304.
23. Z. Z. Sun, A. Lopez and J. Schliemann, *J. Appl. Phys.*, 2011, 109.
24. J. D. Adams, U. Kim and H. T. Soh, *Proc. Natl. Acad. Sci. U. S. A.*, 2008, 105, 18165-18170.
25. F. Shen, H. Hwang, Y. K. Hahn and J. K. Park, *Anal. Chem.*, 2012, 84, 3075-3081.
26. K. Ino, A. Ito and H. Honda, *Biotechnol. Bioeng.*, 2007, 97, 1309-1317.
27. J. B. Tracy and T. M. Crawford, *MRS bulletin*, 2013, 38, 915-920.
28. F. Pirmoradi, L. N. Cheng and M. Chiao, *Journal of Micromechanics and Microengineering*, 2010, 20.
29. F. Fahrni, M. W. J. Prins and L. J. van Ijzendoorn, *J. Magn. Magn. Mater.*, 2009, 321, 1843-1850.
30. H. Bertram and J. Mallinson, *J. Appl. Phys.*, 1970, 41, 1102-1104.
31. H. Bertram and J. Mallinson, *J. Appl. Phys.*, 1969, 40, 1301.
32. A. Lyberatos and R. W. Chantrell, *J. Appl. Phys.*, 1993, 73, 6501-6503.
33. D. Cimpoesu, A. Stancu, I. Klik, C. R. Chang and L. Spinu, *J. Appl. Phys.*, 2011, 109.
34. W. J. Chen, S. F. Zhang and H. N. Bertram, *J. Appl. Phys.*, 1992, 71, 5579-5584.
35. T. Gilbert, *Physical Review*, 1955, 100.
36. T. L. Gilbert, *Magnetics, IEEE Transactions on*, 2004, 40, 3443-3449.
37. J. L. García-Palacios and F. J. Lázaro, *Phys. Rev. B*, 1998, 58, 14937-14958.
38. A. Lyberatos, D. V. Berkov and R. W. Chantrell, *J. Phys.: Condens. Matter*, 1993, 5, 8911-8920.
39. E. Boerner and H. N. Bertram, *Magnetics, IEEE Transactions on*, 1998, 34, 1678-1680.
40. L. Néel, *Ann. géophys*, 1949, 5, 99-136.
41. Y. Nakatani, Y. Uesaka, N. Hayashi and H. Fukushima, *J. Magn. Magn. Mater.*, 1997, 168, 347-351.
42. D. Rodé, H. N. Bertram and D. R. Fredkin, *IEEE T. Magn.*, 1987, 23, 2224-2226.
43. R. Kappiyoor, M. Liangruksa, R. Ganguly and I. K. Puri, *J. Appl. Phys.*, 2010, 108.
44. T. L. Gilbert, *Physical Review*, 1955, 100.
45. P. W. Ma and S. L. Dudarev, *Phys. Rev. B*, 2011, 83.
46. W. F. Brown, *Physical Review*, 1963, 130, 1677.
47. D. V. Berkov and N. L. Gorn, *J. Phys.: Condens. Matter*, 2001, 13, 9369.
48. D. V. Berkov, N. L. Gorn, R. Schmitz and D. Stock, *J. Phys.: Condens. Matter*, 2006, 18, S2595-S2621.
49. M. Azeggagh and H. Kachkachi, *Phys. Rev. B*, 2007, 75.
50. H. B. Callen and T. A. Welton, *Physical Review*, 1951, 83, 34-40.

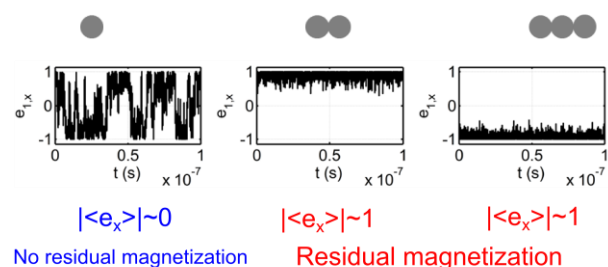
Table of Contents Entry

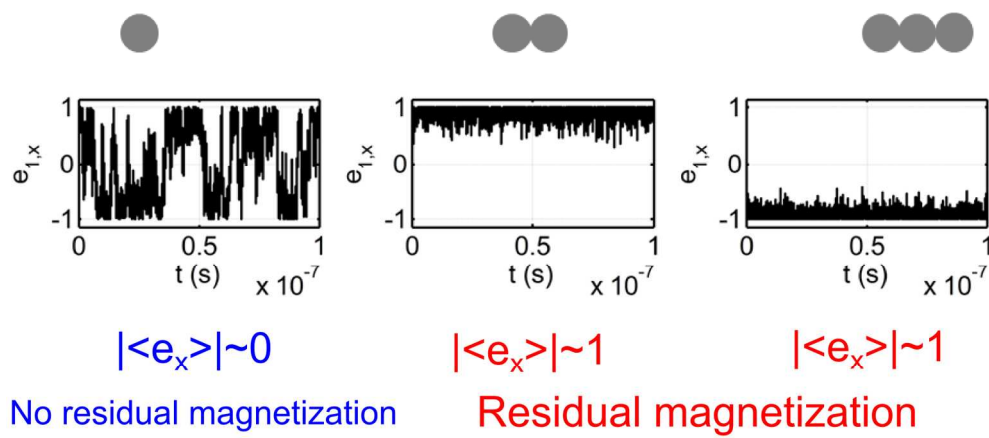
Title: Changing the Magnetic Properties of Microstructure by Directing the Self-assembly of Superparamagnetic Nanoparticles

Authors: Suvojit Ghosh and Ishwar K. Puri

Keywords: superparamagnetism, superferromagnetism, magnetic nanoparticles, emergent properties, micromagnetics, self-assembly

Description: Superparamagnetic nanoparticles that show no individual residual magnetization can be self-assembled into miniature permanent magnets if the particle size and material properties are selected as per the reported design principles.





500x250mm (96 x 96 DPI)